TTC25 Deficiency Results in Defects of the Outer Dynein Arm Docking Machinery and Primary Ciliary Dyskinesia with Left-Right Body Asymmetry Randomization

Julia Wallmeier,[1] Hidetaka Shiratori,[2] Gerard W. Dougherty,[1] Christine Edelbusch,[1] Rim Hjeij,[1] Niki T. Loges,[1] Tabea Menchen,[1] Heike Olbrich,[1] Petra Pennekamp,[1] Johanna Raidt,[1] Claudius Werner,[1] Katsura Minegishi,[2] Kyosuke Shinohara,[2] Yasuko Asai,[2] Katsuyoshi Takaoka,[2] Chanjae Lee,[3] Matthias Griese,[4] Yasin Memari,[5] Richard Durbin,[5] Anja Kolb-Kokocinski,[5] Sascha Sauer,[5,6,7] John B. Wallingford,[3] Hiroshi Hamada,[2] and Heymut Omran[1,*]

Multiprotein complexes referred to as outer dynein arms (ODAs) develop the main mechanical force to generate the ciliary and flagellar beat. ODA defects are the most common cause of primary ciliary dyskinesia (PCD), a congenital disorder of ciliary beating, characterized by recurrent infections of the upper and lower airways, as well as by progressive lung failure and randomization of left-right body asymmetry. Using a whole-exome sequencing approach, we identified recessive loss-of-function mutations within *TTC25* in three individuals from two unrelated families affected by PCD. Mice generated by CRISPR/Cas9 technology and carrying a deletion of exons 2 and 3 in *Ttc25* presented with laterality defects. Consistently, we observed immotile nodal cilia and missing leftward flow via particle image velocimetry. Furthermore, transmission electron microscopy (TEM) analysis in TTC25-deficient mice revealed an absence of ODAs. Consistent with our findings in mice, we were able to show loss of the ciliary ODAs in humans via TEM and immunofluorescence (IF) analyses. Additionally, IF analyses revealed an absence of the ODA docking complex (ODA-DC), along with its known components CCDC114, CCDC151, and ARMC4. Co-immunoprecipitation revealed interaction between the ODA-DC component CCDC114 and TTC25. Thus, here we report TTC25 as a new member of the ODA-DC machinery in humans and mice.

Ciliary motility is important for proper function of diverse processes within the human body.[1] Defects in structure and function of motile respiratory cilia lining the airways lead to the autosomal-recessive mucociliary clearance disorder primary ciliary dyskinesia (PCD [MIM: 244400]), which is clinically characterized by recurrent infections of the upper and lower airways, causing permanent lung damage such as bronchiectasis. About 50% of individuals with PCD exhibit situs inversus due to reduced motility or immotility of node monocilia during early embryogenesis (Kartagener syndrome).[1–3] Defects in the structure of the outer dynein arms (ODAs) are the most common cause of PCD. We utilized homozygosity mapping as well as a whole-exome sequencing (WES) approach to identify candidate genes for PCD. Here, we report that mutations in *TTC25* lead to an ODA-docking complex (ODA-DC) defect involving severely reduced ciliary motility and classical symptoms of PCD, as well as randomization of left-right body asymmetry in humans and mice.

Total genome haplotype data analysis, performed as described previously,[4] in a cohort of PCD-affected individuals with ODA defects revealed a homozygous region on human chromosome 17 in the consanguineous PCD-affected families OP-95 (Figure S1) and OP-1331 (Figure 1), consistent with identity by descent. PCD diagnosis was confirmed by standard clinical diagnostic criteria and documentation of typical symptoms such as neonatal respiratory distress and signs of chronic oto-sinu-pulmonary infections with development of bronchiectasis. Clinical diagnosis included nasal nitric oxide (NO) measurement, medical imaging (X-ray), high-speed video microscopy analysis (HVMA), transmission electron microscopy (TEM), and/or high-resolution immunofluorescence (IF) analysis to analyze ciliary structure and function. We obtained signed and informed consent by using protocols approved by the institutional ethics review board of the University of Muenster.

DNA variants obtained by WES as previously described[5] were filtered according to a recessive disease model. Detailed analyses of all known PCD-associated genes did not reveal any mutations. Genes with monoallelic variants were excluded from further analysis. Furthermore, all variants with an estimated frequency above 0.01 in human variant databases (e.g., 1000 Genomes) were excluded, consistent with models for rare autosomal-recessive diseases. Regions that had shown homozygosity by SNP haplotype data analysis (Affymetrix GeneChip Human Mapping 10K Array v.2.0 and OmniExpressExome 8v.1.2)

[1]Department of Pediatrics, University Hospital Muenster, 48149 Muenster, Germany; [2]Developmental Genetics Group, Graduate School of Frontier Biosciences, Osaka University, Suita, Osaka 565-0871, Japan; [3]Department of Molecular Biosciences, University of Texas at Austin, Austin, TX 78712, USA; [4]Department of Pediatric Pulmonology, Hauner Children's Hospital and Ludwig Maximilian University, The German Center for Lung Research (DZL), 80337 Munich, Germany; [5]Wellcome Trust Sanger Institute, Hinxton, Cambridge CB10 1SA, UK; [6]Berlin Institute for Medical Systems Biology and Berlin Institute of Health Genomics Platforms, Laboratory of Functional Genomics, Nutrigenomics, and Systems Biology, Max Delbrück Center for Molecular Medicine, Robert Rössle Straße 10, 13125 Berlin, Germany; [7]Otto Warburg Laboratory, Max Planck Institute for Molecular Genetics, Ihnestraße 63–73, 14195 Berlin, Germany
*Correspondence: heymut.omran@ukmuenster.de
http://dx.doi.org/10.1016/j.ajhg.2016.06.014.
© 2016 American Society of Human Genetics.

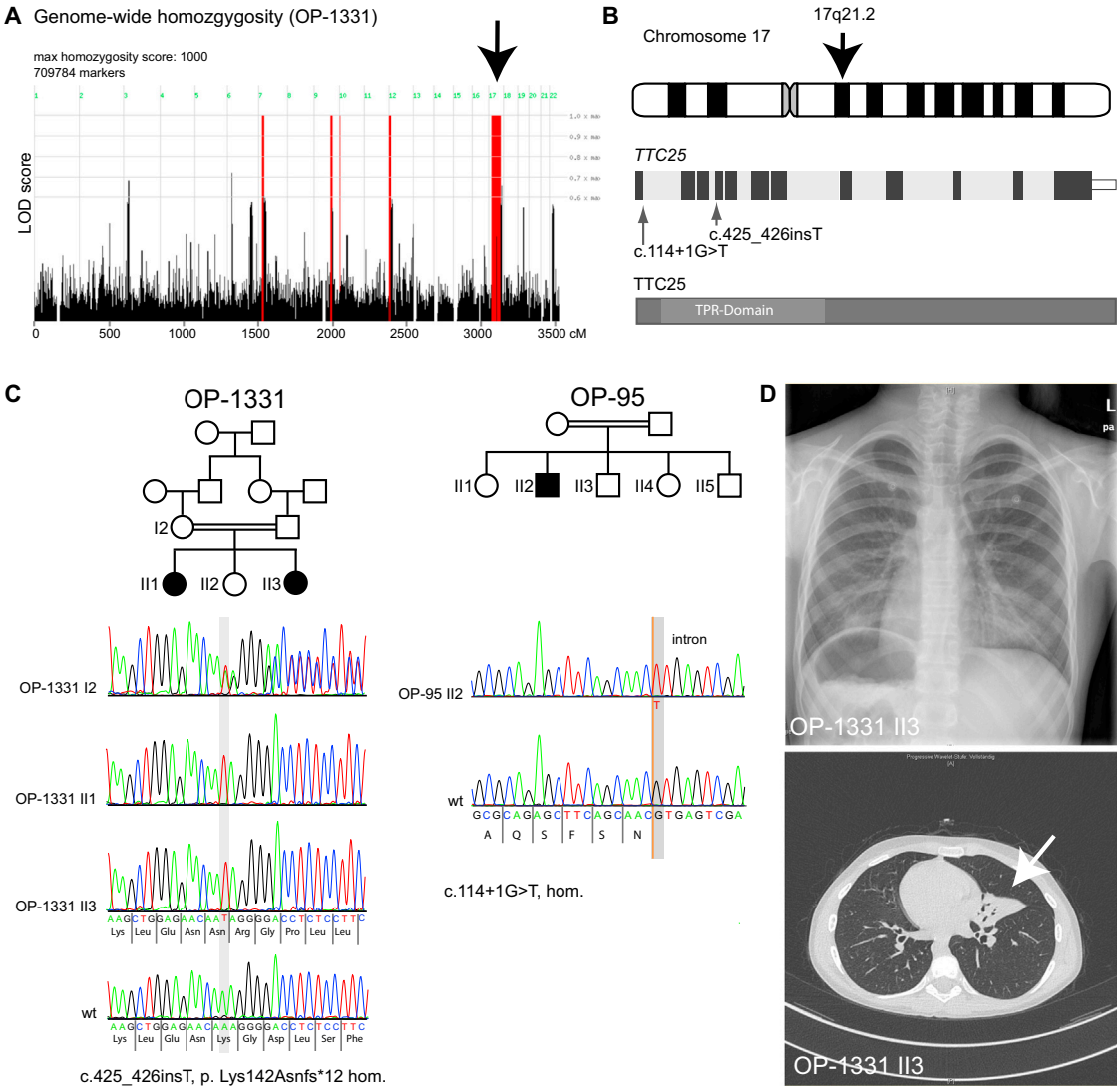

Figure 1. Mutations in *TTC25* Cause PCD
(A) Genome-wide homozygosity SNP studies in individuals OP-1331 II1 and OP-1331II3 revealed a large (50 Mb) homozygous region on chromosome 17, spanning the *TTC25* locus (black arrow).
(B) We identified two homozygous loss-of-function mutations in *TTC25* in the two unrelated consanguineous PCD-affected families OP-95 and OP-1331. *TTC25* encodes a tetratricopeptide (TPR)-domain containing protein.
(C) The homozygous splice-site mutation (c.114+1G>T) disrupts the evolutionarily conserved canonical donor site in OP-95 II2. The homozygous frameshift mutation (c.425_426insT) was identified in the two affected siblings II1 and II3 of family OP-1331. Consistent with autosomal-recessive inheritance, the mutation was detected in the heterozygous state in the mother (OP-1331 I2).
(D) The PCD-affected individual OP-1331 II3 had situs inversus, documented by chest X-ray (upper panel) and computed tomography of the thorax (CT-scan; lower panel). Please also note complete atelectasis of the left-positioned middle lobe, as well as bronchiectasis (white arrow).

were analyzed for possible PCD-causing variants coding for non-synonymous or splice-site substitutions as well as small insertions and/or deletions (indels) (Tables S1 and S2). This analysis revealed a homozygous splice-site mutation (c.114+1G>T) in individual OP-95 II2 and a homozygous out-of-frame insertion (c.425_426insT [p.Lys142Asnfs*12]) in OP-1331 II1 in *TTC25* (GenBank: NM_031421), predicting early termination of translation. The mutations were confirmed by Sanger sequencing, as previously described.[6] Segregation analysis was performed in family OP-1331, confirming that the mutation segregated consistent with an autosomal-recessive inheritance pattern (Figure 1). Overall, classical loss-of-function *TTC25* mutations were identified in three PCD-affected individuals from two families (Figure 1).

All three PCD-affected individuals (OP-95 II2, OP-1331 II1, and OP-1331 II3) displayed typical clinical PCD phenotypes, including recurrent upper (chronic rhinitis, chronic otitis, chronic sinusitis, and nasal polyps) and lower (chronic productive cough, recurrent pneumonia, and bronchiectasis) airway disease (Figure 1). OP-1331 II1 presented with respiratory distress after birth. Nasal NO

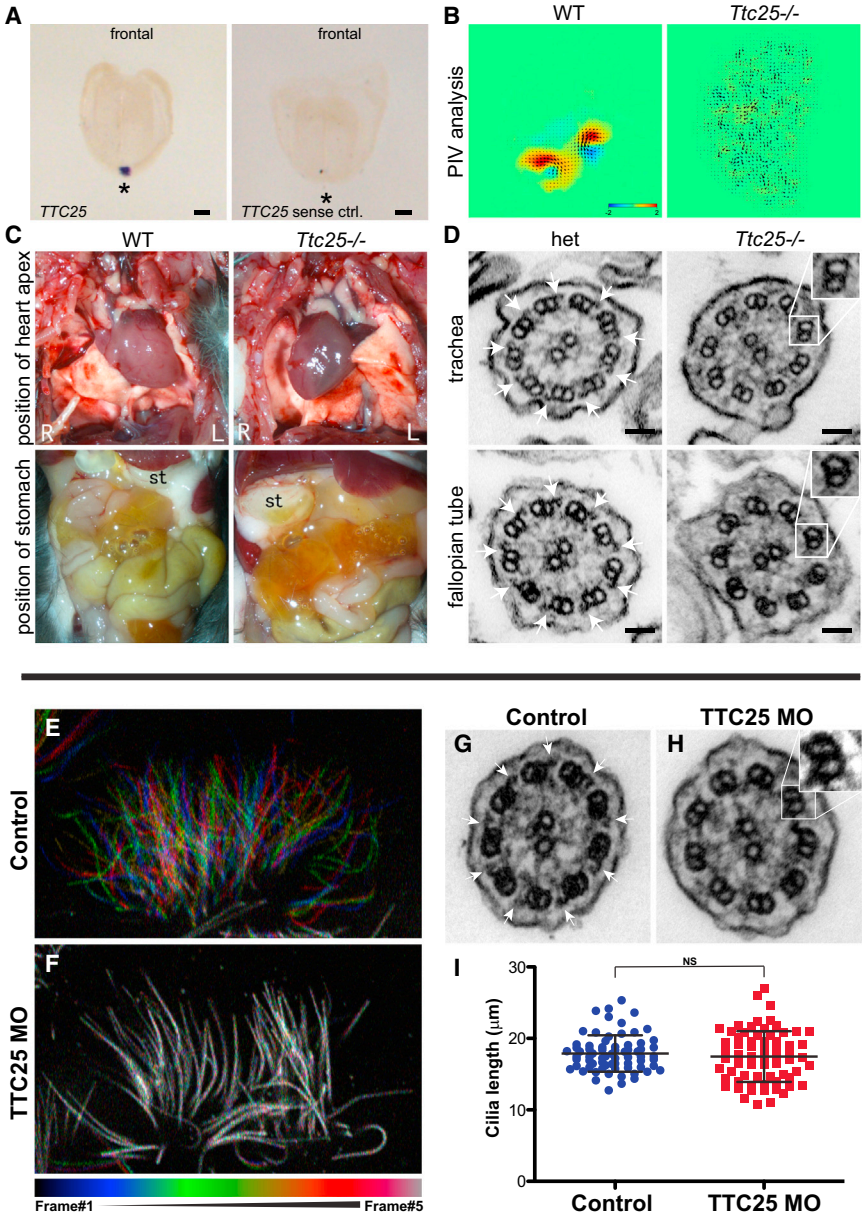

Figure 2. Analysis of *Ttc25* Mutant Mice and Ttc25 Knockdown in *Xenopus*

(A) In situ hybridization analyses of wild-type mouse embryos at the age of embryonic day (E) 7.5 revealed strong and restricted expression of *Ttc25* at the ventral node (asterisk). A sense probe was used for negative controls, which do not show any signal (right).

(B) Particle image velocimetry (PIV) analysis of the ventral node also revealed differences between wild-type (WT) and mutant embryos. Whereas, at the wild-type node, flow of particles is rapid and directed, for the *Ttc25* mutant embryo, only scattered and undirected movement could be observed. Leftward flow is shown in yellow and red and rightward in blue.

(C) Mice carrying the *Ttc25* mutation show randomization of left-right body asymmetry. In wild-type mice, the heart apex points to the left side (top left). In mutant mice, shown here, it points to the right side (dextrocardia) (top right). The stomach (st) is localized on the left side in wild-type animals (bottom left), but was found on the right side in *Ttc25* mutants (bottom right).

(D) Transmission electron microscopy (TEM) of ciliary cross-sections from the trachea (upper panel) or fallopian tubes (lower panel) of a heterozygous (het) *Ttc25* mutant mouse (left column) revealed the presence of ODAs (white arrows) attached to the A tubules. In homozygous *Ttc25* mutant mice (right column), the ODAs are lacking.

(E and F) Color-based time coding of time-lapse data from high-speed confocal microscopy reveals robust beating in control multiciliated cells of *Xenopus* (E), and a failure of beating in *Ttc25* morphants (F). Colored bar below indicates the color of each of five frames in the time-lapse movie.

(G–I) ODAs are apparent in TEM of normal axonemes of *Xenopus* multiciliated cells (G), but are absent in axonemes after *Ttc25* knockdown (H). At the stages examined here, *Ttc25* knockdown has no effect on cilium length (I).

Scale bars represent 100 μm (ISH) and 5 nm (TEM).

production rate was below 100 nL/min, consistent with the diagnosis of PCD.[7] Two individuals displayed laterality defects: OP-1331 II3 presented with situs inversus and OP-95 II2 had situs ambiguous. In one individual (OP-1331 II1), situs solitus was present, indicating that *TTC25* mutations result in PCD and randomization of left-right body asymmetry.

TTC25 is located on human chromosome 17q21.2 and comprises 12 exons. The 2.255-bp *TTC25* cDNA encodes the 672-amino-acid tetratricopeptide repeat domain-containing protein 25. TTC25 contains eight tetratricopeptide (TPR) domains, which exist in organisms from bacteria to humans and are known to be involved in multiprotein-complex formation.[8]

To further analyze the molecular function of TTC25, we designed a mouse model via CRIPSR/Cas9 that carries a deletion of *Ttc25* exons 2 and 3 (Figure S2). Homozygous *Ttc25* mutants phenotypically exhibited several differences from wild-type mice, consistent with previous findings in mice carrying mutations in genes related to ciliary motility[9] (Figure 2, Table S1). Most mice presented with small body size and some with hydrocephalus at the age of 2 weeks. Consistent with our findings in PCD-affected individuals, most mutant animals displayed a variety of left-right body asymmetry defects, including reversal of lung lobation or dextrocardia (Figure 2), consistent with the laterality defects observed previously after *Ttc25* knockdown in *Xenopus*.[10]

Analysis of the genotype frequency of heterozygous intercrosses revealed deviation from the Mendelian distribution (Table S2). At examination 2 weeks after birth, only 6 out of 53 born mice (11.3%) carried the homozygous *Ttc25* mutation, thus a lower percentage of homozygous *Ttc25* mutant animals was counted than suspected. We therefore hypothesized that some *Ttc25* mutant mice died prenatally due to severe laterality defects.

To better understand the functional role of TTC25 in the development of left-right asymmetry, we analyzed *Ttc25* expression during early embryonic development by whole-mount in situ hybridization. Analyzing wild-type mouse embryos with probes directed against *Ttc25* mRNA, we observed a well-defined signal restricted to the ventral node, the left-right organizer, where motile monocilia play an important functional role during the critical period of left-right determination (Figure 2A). Next, we studied the monocilia at the left-right organizer. First, we noticed immotility of monocilia at the node of homozygous *Ttc25* mutants (Movies S1 and S2). To check whether the node monocilia in the mutants were capable of generating the leftward-directed nodal flow necessary for determination of left-right asymmetry, we analyzed the embryos by particle image velocimetry (PIV) (Figure 2B), applying particles to the cavity of the node to observe their transport through the nodal pit. Whereas in wild-type embryos the nodal cilia generated a strong, mainly leftward-directed flow, in the mutant embryo, the particles moved only diffusely. This strongly indicates that the cilia are not capable of generating directed fluid flow sufficient for proper axis development. Our results in mice suggest that TTC25 plays an essential role in the correct function of motile cilia at the ventral node and is therefore important for the development of left-right body asymmetry.

Next, we analyzed the subcellular localization of TTC25 in human respiratory cells obtained by nasal brush biopsy in healthy control individuals. High-resolution IF microscopy was performed with anti-TTC25 antibody (ab157630, 1:500) as previously reported[11] and demonstrated TTC25 localization throughout the ciliary axonemes (Figure 3A), consistent with previous findings in multiciliated cells (MCCs) of *Xenopus* skin.[12] In agreement with the predicted loss-of-function mutations in the three PCD-affected individuals (OP-95 II2, OP-1331 II1, and OP-1331 II3), TTC25 was not detectable in mutant ciliary axonemes (Figures 3B and 3D).

To further characterize the functional consequences of recessive *TTC25* mutations, we performed TEM (OP-1331 II1 and OP-1331 II3) and HVMA[13] of the ciliary beat (OP-95 II2, OP-1331 II1, and OP-1331 II3) in respiratory epithelial cells obtained by nasal brush biopsy. Motile respiratory cilia consist of multiprotein complexes serving different functions. Careful ultrastructural analyses showed that *TTC25* mutant ciliary axonemes had a normal 9+2 architecture and no evidence of tubular disorganization. Cross-sections of *TTC25* mutant respiratory cilia revealed absence of ODAs, which are easily depicted in respiratory cilia of control individuals (Figure 4A). The ODAs generate the main mechanical force by converting chemical energy of ATP, by transient binding of neighboring microtubules and conformational changes. Consistent with defective ODA function, we found cilia to be immotile in ciliated respiratory cells from PCD-affected individuals OP-95 II2, OP-1331 II1, and OP-1331 II3. In only a few cells, some residual flickery ciliary movement was visible by HVMA (Movies S3–S5), consistent with defective ODA function.[13] Interestingly, we did not observe any signs of fewer or shortened cilia in the respiratory epithelial cells of individuals with a *TTC25* mutation. Previous studies of morpholino knockdown of *Ttc25* in *Xenopus* resulted in fewer cilia, which appeared very short via scanning electron microscopy.[12] Therefore, it was speculated that TTC25 might play a role as a ciliogenesis factor. Here, we do not have any evidence for cilia reduced in either length or number. As observed in the respiratory cilia of humans carrying recessive mutations in *TTC25*, TEM analyses of the trachea and fallopian tubes of *Ttc25* mutant mice revealed an absence of ODAs from the ciliary axonemes, which are present in the heterozygous controls (Figure 2D). Consistent with the absence of the ODAs, video microscopy of tracheal tissue confirmed a severe reduction of cilia beating. There was no evidence of short cilia or a reduction in number, consistent with the findings in humans.

In light of these data, we revisited the knockdown phenotype in *Xenopus* MCCs. memGFP mRNA synthesized with an mMESSAGE mMACHINE kit (Ambion) and *TTC25* morpholino (Gene Tools) were injected into two ventral cells of four-cell-stage *Xenopus* embryos. We found that defects in ciliogenesis[12] were apparent only at early stages, whereas more mature MCCs displayed normal cilium length after *Ttc25* knockdown (Figure 2I). However, in these later stages, high-speed confocal microscopy revealed severe defects in ciliary beating in morphant MCCs (Figures 2E and 2F, Movies S6 and S7). *Ttc25* morphant cilia in *Xenopus* retained a twitching motility (severe defect in organized beating), similar to that described above for human MCCs (Movies S6 and S7). Finally, TEM analysis revealed a specific loss of ODAs in *Ttc25* morphants (Figures 2G and 2H), consistent with our findings in human individuals with *TTC25* mutations.

ODAs, arranged in a 24 nm repeat along the A tubule, are multiprotein complexes composed of dynein heavy chains (HCs, 400–500 kDa), intermediate chains (ICs, 45–140 kDa), and light chains (LCs, 8–28 kDa).[1] We have previously shown that in contrast to *Chlamydomonas* flagella, ODA complexes vary in their composition of HCs along the human respiratory ciliary axoneme. At least two different types of ODAs are present in human respiratory cilia. Whereas type 1 ODAs (ODA HC DNAH9 negative and ODA HC DNAH5 positive) are present in the proximal part of the ciliary axonemes, type 2 ODAs (ODA HC DNAH5 positive and ODA HC DNAH9 positive) are distributed in the distal region of the axonemes.[11] To

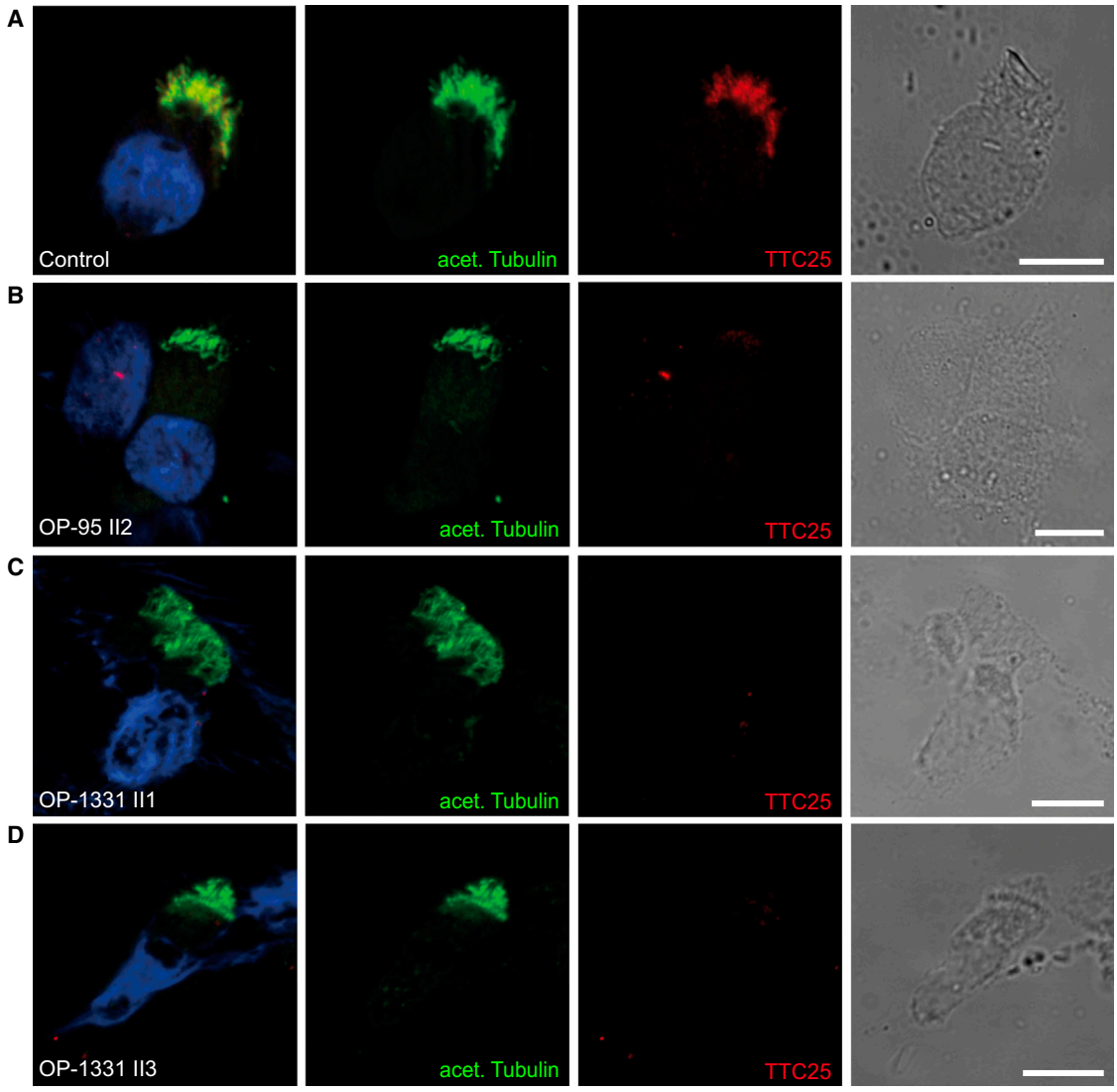

Figure 3. Axonemal Localization of TTC25
(A) In respiratory cells obtained from a healthy control individual, TTC25 (red) localizes throughout the ciliary axoneme, which is marked by acetylated tubulin (green). This co-localization is represented by yellow in the merged image.
(B–D) TTC25 is absent in respiratory cells from individuals harboring recessive loss-of-function *TTC25* mutations. Absence of TTC25 protein localization in the affected individuals OP-95 II2 (B), OP-1331 II1 (C), and OP-1331 II3 (D) is consistent with the detected loss-of-function mutations (c.114+1G>T and c.425_426insT) and confirms specificity of the polyclonal anti-TTC25 antibody (Abcam, ab157630, 1:500). The nucleus (blue) was stained with Hoechst33342 (Sigma, 14533-100MG, 1:1000).
Scale bars represent 10 μm.

further characterize the ODA defect in *TTC25* mutant respiratory cells on the sub-cellular level, we performed high resolution IF analysis with antibodies directed against the ODA HCs DNAH5 and DNAH9 as previously described[11] in individuals OP-95 II2, OP-1331 II1, and OP-1331 II3. Consistent with an ODA defect affecting both ODA types, the ODA HCs DNAH5 and DNAH9 were completely absent from the ciliary axonemes of *TTC25* mutant respiratory cilia (Figures 4B and 4C).

ODAs are pre-assembled in the cytoplasm by the cytoplasmic-dynein-arm assembly machinery, which comprises several components that are predicted to localize to the cytoplasm, such as dynein axonemal assembly factors (DNAAFs).[14,15] Thus, based on the axonemal localization of TTC25, it is highly unlikely that TTC25 functions as a cytoplasmic-dynein-arm assembly factor. In addition, mutations in genes encoding cytoplasmic pre-assembly factors not only cause defects of ODAs, but also of inner dynein arms (IDAs), which are supposed to modulate the waveform of the beating. To distinguish between an isolated ODA defect and a combined defect of ODAs and IDAs, we performed IF with antibodies directed against the IDA LC DNALI1,[16] which is absent from ciliary axonemes with cytoplasmic pre-assembly defects.[14] The preservation of DNALI1 in *TTC25* mutant cilia makes a defect related to cytoplasmic-dynein-arm pre-assembly very unlikely (Figure 4D). Because genetic defects responsible for ODA defects do not result in

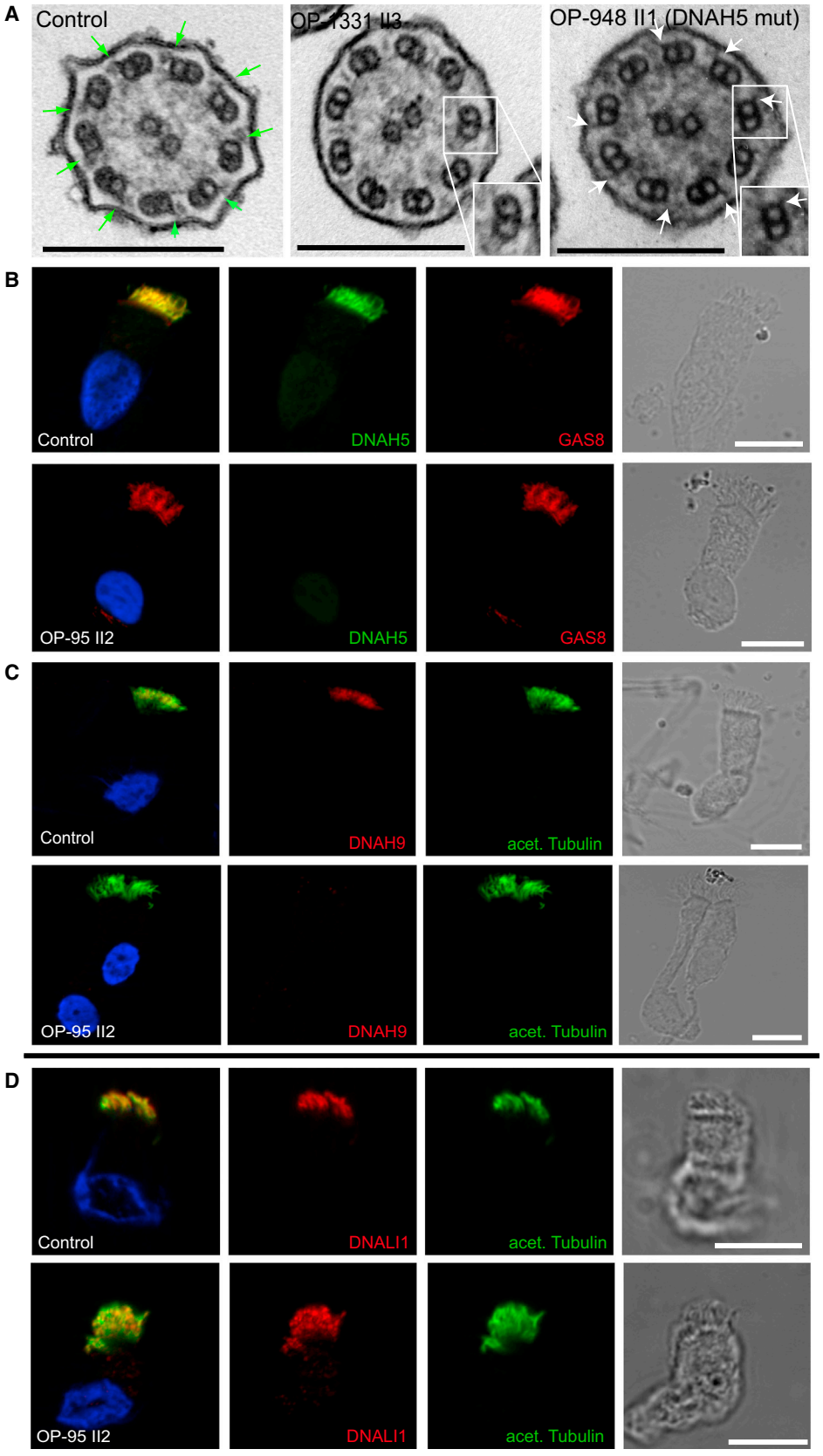

Figure 4. Mutations in *TTC25* Result in Ultrastructural Defects of the ODAs Detectable by TEM and IF Analysis in Ciliated Respiratory Cells

(A) TEM analyses of OP-1331 II1 (not shown) and OP-1331 II3 demonstrate absence of ODAs, which are present in control cilia (green arrows). Interestingly, by comparing TEM cross-sections of OP-1331II1 and OP-1331 II3 with the TEM cross sections of OP-948 II1

(legend continued on next page)

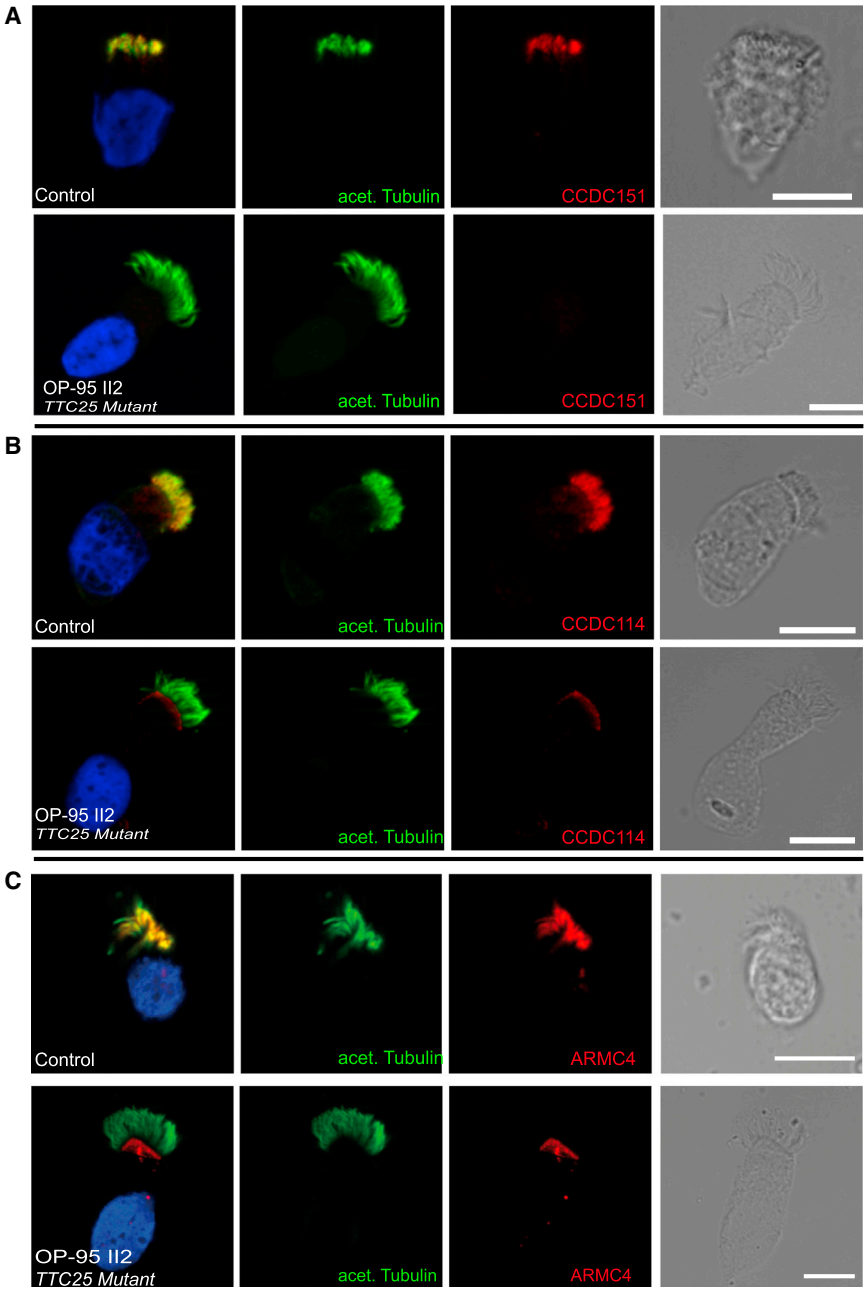

Figure 5. TTC25 Functions in the Docking of ODAs in Respiratory Ciliary Axonemes

Respiratory epithelial cells from an unaffected control individual and from OP-95 II2, carrying *TTC25* mutations, were double-labeled with antibodies directed against acetylated tubulin (green) and the ODA-DC components CCDC151 (Atlas Antibodies, HPA04418, 1:250) (red, A), CCDC114 (Atlas Antibodies, HPA042524, 1:500) (red, B), or ARMC4 (Atlas Antibodies, HPA037829, 1:500) (red, C). Yellow shows co-localization of CCDC151, CCDC114, or ARMC4 with acetylated tubulin in control axonemes (upper panels in A, B, and C). However CCDC151, CCDC114, and ARMC4 are absent from the ciliary axonemes of *TTC25* mutant cells (lower panels in A, B, and C). The red signal, which is still visible in ARMC4- and CCDC114-deficient cells, is probably related to the unspecific binding of the polyclonal antibodies to the basal bodies and is probably not related to residual CCDC114 or ARMC4 within the cilia. The nuclei (blue) were stained with Hoechst33342 (Sigma, 14533-100MG, 1:1,000). Scale bars represent 10 μm.

abnormalities of the radial spokes, which connect the central single tubules with the outer doublets, or the nexin links, connecting the outer doublets, we studied the localization of the nexin-dynein regulatory complex (N-DRC) component GAS8[17] (Figure 4B), as well as the radial spoke head protein RSPH4A[5] (data not shown). As expected, we did not detect any abnormalities within these structures.

ODAs require a docking complex facilitating their docking on the microtubule.[18,19] Interestingly, when comparing TEM cross-sections from OP-1331 II3 with the TEM cross sections from OP-948 II1 carrying loss-of-function mutations in *DNAH5* (MIM: 608644), we observed that the cells of OP-1331 II3 also lack the tiny projections on the doublet microtubules known to represent the ODA-DC (Figure 4A). This indicates that *TTC25* mutations lead to a combined ODA and ODA-DC defect. Consistent with the findings in humans, TEM analysis in the mutant mice also revealed missing ODA-DCs. Given that TEM analysis revealed the absence of ODA-DCs in *TTC25* and *Ttc25* mutant cells (Figures 2 and 4), we next studied the localization of the known proteins associated with docking of the

carrying loss-of-function mutations in *DNAH5*, we could observe that the cells of OP-1331 II1 and OP-1331 II3 also lack the tiny projections on the doublet microtubules known to represent the ODA-DC that can still be detected in *DNAH5* mutant cilia (white arrows). This indicates that *TTC25* mutations lead to a combined ODA and ODA-DC defect.

(B and C) IF analyses confirm absence of the ODA HC DNAH5[14] (green, OP-95 II2) (B) and absence of the ODA HC DNAH9[14] (red, OP-95 II2) (C).

(D) The localization of the IDA LC DNALI1[14] (red) is not altered in mutant respiratory cells (OP-95 II2).

Yellow represents co-localization of DNAH5 (green, B) with GAS8 (Atlas Antibodies, HPA041311, 1:500) (N-DRC component; red, B), DNAH9 (red, C) and DNALI1 (red, D) with acetylated tubulin (green, C and D). Nuclei (blue) were stained with Hoechst33342 (Sigma, 14533-100MG, 1:1,000). Scale bars represent 10 μm.

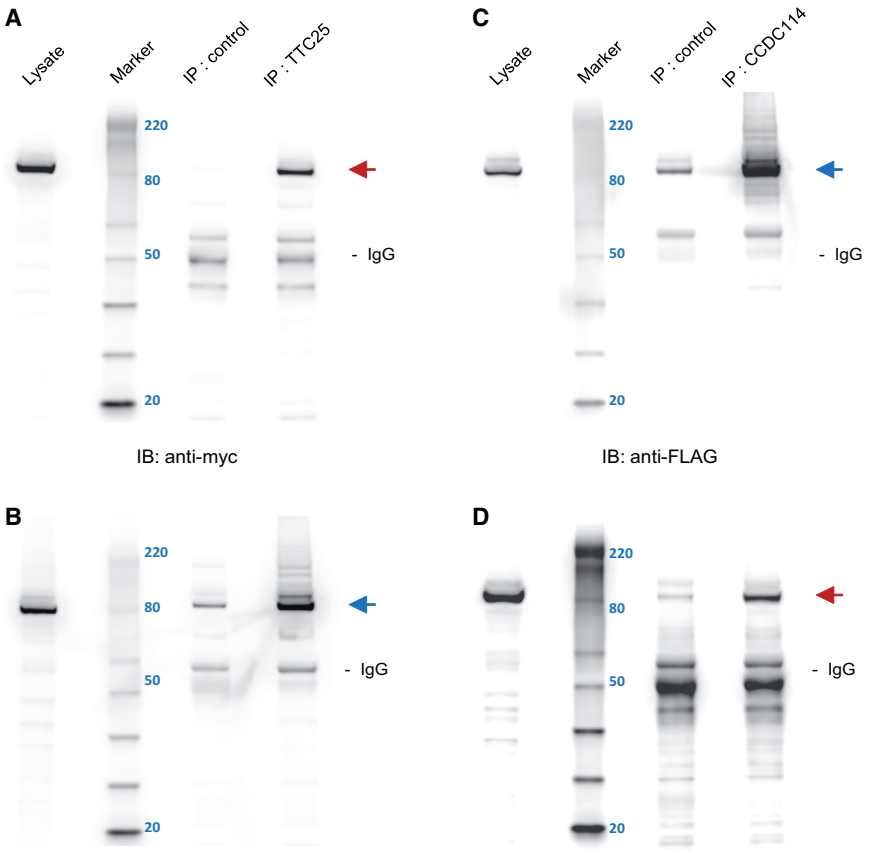

Figure 6. TTC25 Reciprocally Co-immunoprecipitates with the ODA-DC Protein CCDC114

Following co-expression of myc-tagged TTC25 and FLAG-tagged CCDC114 in HEK293 cells, lysates were immunoprecipitated with rabbit control and either rabbit anti-TTC25 or rabbit anti-CCDC114 antibodies.

(A and B) Rabbit anti-TTC25 immunoprecipitates myc-tagged TTC25 (red arrow) and FLAG-tagged CCDC114 (blue arrow), as detected by immunoblotting (IB) with mouse anti-myc (Abcam, ab18185, 1:2000) and anti-FLAG (Sigma, F1804, 1:2000) antibodies.

(C and D) Rabbit anti-CCDC114 immunoprecipitates FLAG-tagged CCDC114 (blue arrow) and myc-tagged TTC25 (red arrow), as detected by immunoblotting with mouse anti-myc and anti-FLAG antibodies. Relative molecular weight in kDa is visualized with a Magic Mark XP protein ladder and indicated by blue numerals (Marker). Lysate equals approximately 25 μg of protein. Immunoprecipitate fractions represent 1/16 lysis volume (33 μl); 16 μl of immunoprecipitate were electrophoresed. Immunoreactive bands in the range of 50 kDa most likely indicate HC IgG. The estimated molecular weights of TTC25 (77 kDa) and CCDC114 (75 kDa) are slightly higher due to additional peptide sequence from myc and FLAG epitopes, respectively. Residual immunoreactivity in control lanes most likely represents non-specific binding of overexpressed proteins to protein agarose A beads. Normal rabbit IgG (Santa Cruz Biotechnology, sc-2027) was used as control for immunoprecipitations.

ODAs, CCDC114, ARMC4, and CCDC151, as previously reported,[20] in respiratory epithelial cells obtained from individuals with mutations in *TTC25*. Indeed, we found that *TTC25* mutant cilia lack any detectable CCDC151, CCDC114, or ARMC4 (Figure 5). This indicates that TTC25 is essential for the assembly of all three known ODA-DC proteins. However, TTC25 could still localize to the axonemes of cells deficient in ODA HC DNAH5, as well as to the cells of individuals with mutations in genes encoding CCDC114, CCDC151 and ARMC4 (Figure S3). Thus, we identified TTC25 as a new member involved in the ODA-DC-associated machinery.

We cloned the full-length human *TTC25* isoform from RNA of healthy respiratory epithelial cells and determined that anti-TTC25 antibodies could detect TTC25 ectopically expressed in HEK293 cells by both western blotting and immunoprecipitation (data not shown), supporting the specificity of anti-TTC25 IF analysis (Figure 3). We therefore tested whether TTC25 interacts with ODA-DC components. As shown in Figure 6, myc-tagged TTC25 reciprocally co-immunoprecipitated with FLAG-tagged CCDC114, using anti-TTC25 for immunoprecipitation. We previously demonstrated a direct interaction between ODA-DCs CCDC114 and CCDC151 by yeast two-hybrid and reciprocal co-immunoprecipitation.[19] Because CCDC114, CCDC151, and ARMC4 are all absent in *TTC25* mutant ciliary axonemes, we propose that TTC25 facilitates recruitment and/or attachment of these ODA-DC proteins to ciliary axonemes via interaction with CCDC114 (Figure 6).

Consistent with our findings that TTC25 plays a functional role in ODA docking, immune gold electron microscopy studies in sea urchins have shown that the TTC25 ortholog AP58 localizes periodically in ~25 nm intervals along sperm flagella, coinciding with the repeat of the ODA.[21]

The ODA-DC machinery has been well studied in the green unicellular alga *Chlamydomonas*. Interestingly, TTC25 is not present in the *Chlamydomonas* genome, suggesting it evolved in higher eukaryotes. Here, we report TTC25 as a new member of the ODA-DC machinery. ODAs are pre-assembled in the cytoplasm[22] and then delivered by the intraflagellar transport (IFT) machinery[23] to the ODA docking sites. Because recent studies have found interactions between the IFT machinery and Ttc25 in zebrafish,[24] as well as between the IFT machinery and CCDC151 in flies[20] and humans,[25] we hypothesize that TTC25 might functionally link the IFT system to the ODA-DC and ODA HC machinery in motile cilia. Alternatively, it might serve as a link of the ODA-DC to the microtubules.

The identification and detailed molecular characterization of a ODA-DC defect responsible for primary ciliary dyskinesia will aid diagnosis and help to develop therapeutic strategies.

Supplemental Data

Supplemental Data include three figures, four tables, and seven movies and can be found with this article online at http://dx.doi.org/10.1016/j.ajhg.2016.06.014.

Acknowledgments

We thank the affected individuals and their families for participating in this study. We thank C. Westermann from the Pathology Department of the University of Muenster for electron microscopy assistance. We thank M. Herting, S. Helms, B. Lechtape, L. Overkamp, A. Robbers, and F.-J. Seesing for their technical assistance. Furthermore, we thank Y. Ikawa for maintaining the mutant mouse and Y. Uegaki and H. Nishimura for the help in generating and maintaining the mutant mouse. We also thank K. Okamoto (University of Tokyo) for providing the PIV analysis software. This work was funded by the Deutsche Forschungsgemeinschaft (Om6/4, Om6/7, and Om6/8 to H. Omran and OL450/1 to H. Olbrich). Furthermore, this study was supported by the European Commission (FP7/2007-2013, under grant agreement number 262055 [ESGI], as a Transnational Access project of the European Sequencing and Genotyping Infrastructure), the Interdisziplinaeres Zentrum für Klinische Forschung Muenster (Om2/009/12 and Om2/015/16 to H. Omran), BESTCILIA (under grant agreement number 305404), the Schroeder Stiftung (H. Omran), Kindness for Kids (H. Omran), and the Innovative Medizinische Forschung (WA 1 2 14 18 to J.W. and LO 1 2 15 17 to N.T.L.), as well as by CREST, Japan Science and Technology Agency (project no. 13417760), and the Japan Society for the Promotion of Science (project no. 24113004) to H.H. C.L. and J.B.W. were supported by funding from the US National Heart, Lung, and Blood Institute (HL117164). R.D. and A.K-K. were supported by Wellcome Trust grant WT098051.

Received: April 6, 2016
Accepted: June 17, 2016
Published: August 4, 2016

Web Resources

GenBank, http://www.ncbi.nlm.nih.gov/genbank/
OMIM, http://www.omim.org/

References

1. Fliegauf, M., Benzing, T., and Omran, H. (2007). When cilia go bad: cilia defects and ciliopathies. Nat. Rev. Mol. Cell Biol. *8*, 880–893.
2. Afzelius, B.A. (1976). A human syndrome caused by immotile cilia. Science *193*, 317–319.
3. Pennekamp, P., Menchen, T., Dworniczak, B., and Hamada, H. (2015). Situs inversus and ciliary abnormalities: 20 years later, what is the connection? Cilia *4*, 1.
4. Olbrich, H., Schmidts, M., Werner, C., Onoufriadis, A., Loges, N.T., Raidt, J., Banki, N.F., Shoemark, A., Burgoyne, T., Al Turki, S., et al.; UK10K Consortium (2012). Recessive HYDIN mutations cause primary ciliary dyskinesia without randomization of left-right body asymmetry. Am. J. Hum. Genet. *91*, 672–684.
5. Frommer, A., Hjeij, R., Loges, N.T., Edelbusch, C., Jahnke, C., Raidt, J., Werner, C., Wallmeier, J., Große-Onnebrink, J., Olbrich, H., et al. (2015). Immunofluorescence Analysis and Diagnosis of Primary Ciliary Dyskinesia with Radial Spoke Defects. Am. J. Respir. Cell Mol. Biol. *53*, 563–573.
6. Tarkar, A., Loges, N.T., Slagle, C.E., Francis, R., Dougherty, G.W., Tamayo, J.V., Shook, B., Cantino, M., Schwartz, D., Jahnke, C., et al.; UK10K (2013). DYX1C1 is required for axonemal dynein assembly and ciliary motility. Nat. Genet. *45*, 995–1003.
7. Collins, S.A., Gove, K., Walker, W., and Lucas, J.S.A. (2014). Nasal nitric oxide screening for primary ciliary dyskinesia: systematic review and meta-analysis. Eur. Respir. J. *44*, 1589–1599.
8. Zeytuni, N., and Zarivach, R. (2012). Structural and functional discussion of the tetra-trico-peptide repeat, a protein interaction module. Structure *20*, 397–405.
9. Ibañez-Tallon, I., Gorokhova, S., and Heintz, N. (2002). Loss of function of axonemal dynein Mdnah5 causes primary ciliary dyskinesia and hydrocephalus. Hum. Mol. Genet. *11*, 715–721.
10. Chung, M.-I., Peyrot, S.M., LeBoeuf, S., Park, T.J., McGary, K.L., Marcotte, E.M., and Wallingford, J.B. (2012). RFX2 is broadly required for ciliogenesis during vertebrate development. Dev. Biol. *363*, 155–165.
11. Fliegauf, M., Olbrich, H., Horvath, J., Wildhaber, J.H., Zariwala, M.A., Kennedy, M., Knowles, M.R., and Omran, H. (2005). Mislocalization of DNAH5 and DNAH9 in respiratory cells from patients with primary ciliary dyskinesia. Am. J. Respir. Crit. Care Med. *171*, 1343–1349.
12. Hayes, J.M., Kim, S.K., Abitua, P.B., Park, T.J., Herrington, E.R., Kitayama, A., Grow, M.W., Ueno, N., and Wallingford, J.B. (2007). Identification of novel ciliogenesis factors using a new in vivo model for mucociliary epithelial development. Dev. Biol. *312*, 115–130.
13. Raidt, J., Wallmeier, J., Hjeij, R., Onnebrink, J.G., Pennekamp, P., Loges, N.T., Olbrich, H., Häffner, K., Dougherty, G.W., Omran, H., and Werner, C. (2014). Ciliary beat pattern and frequency in genetic variants of primary ciliary dyskinesia. Eur. Respir. J. *44*, 1579–1588.
14. Omran, H., Kobayashi, D., Olbrich, H., Tsukahara, T., Loges, N.T., Hagiwara, H., Zhang, Q., Leblond, G., O'Toole, E., Hara, C., et al. (2008). Ktu/PF13 is required for cytoplasmic pre-assembly of axonemal dyneins. Nature *456*, 611–616.
15. Loges, N.T., Olbrich, H., Becker-Heck, A., Häffner, K., Heer, A., Reinhard, C., Schmidts, M., Kispert, A., Zariwala, M.A., Leigh, M.W., et al. (2009). Deletions and point mutations of LRRC50 cause primary ciliary dyskinesia due to dynein arm defects. Am. J. Hum. Genet. *85*, 883–889.
16. Rashid, S., Breckle, R., Hupe, M., Geisler, S., Doerwald, N., and Neesen, J. (2006). The murine Dnali1 gene encodes a flagellar protein that interacts with the cytoplasmic dynein heavy chain 1. Mol. Reprod. Dev. *73*, 784–794.
17. Olbrich, H., Cremers, C., Loges, N.T., Werner, C., Nielsen, K.G., Marthin, J.K., Philipsen, M., Wallmeier, J., Pennekamp, P., Menchen, T., et al. (2015). Loss-of-Function GAS8 Mutations Cause Primary Ciliary Dyskinesia and Disrupt the Nexin-Dynein Regulatory Complex. Am. J. Hum. Genet. *97*, 546–554.
18. Takada, S., and Kamiya, R. (1994). Functional reconstitution of Chlamydomonas outer dynein arms from alpha-beta and

gamma subunits: requirement of a third factor. J. Cell Biol. *126*, 737–745.

19. Hjeij, R., Onoufriadis, A., Watson, C.M., Slagle, C.E., Klena, N.T., Dougherty, G.W., Kurkowiak, M., Loges, N.T., Diggle, C.P., Morante, N.F.C., et al.; UK10K Consortium (2014). CCDC151 mutations cause primary ciliary dyskinesia by disruption of the outer dynein arm docking complex formation. Am. J. Hum. Genet. *95*, 257–274.
20. Jerber, J., Baas, D., Soulavie, F., Chhin, B., Cortier, E., Vesque, C., Thomas, J., and Durand, B. (2014). The coiled-coil domain containing protein CCDC151 is required for the function of IFT-dependent motile cilia in animals. Hum. Mol. Genet. *23*, 563–577.
21. Ogawa, K., and Inaba, K. (2006). Ap58: a novel in situ outer dynein arm-binding protein. Biochem. Biophys. Res. Commun. *343*, 385–390.
22. Fowkes, M.E., and Mitchell, D.R. (1998). The role of preassembled cytoplasmic complexes in assembly of flagellar dynein subunits. Mol. Biol. Cell *9*, 2337–2347.
23. Hou, Y., Qin, H., Follit, J.A., Pazour, G.J., Rosenbaum, J.L., and Witman, G.B. (2007). Functional analysis of an individual IFT protein: IFT46 is required for transport of outer dynein arms into flagella. J. Cell Biol. *176*, 653–665.
24. Xu, Y., Cao, J., Huang, S., Feng, D., Zhang, W., Zhu, X., and Yan, X. (2015). Characterization of tetratricopeptide repeat-containing proteins critical for cilia formation and function. PLoS ONE *10*, e0124378.
25. Huttlin, E.L., Ting, L., Bruckner, R.J., Gebreab, F., Gygi, M.P., Szpyt, J., Tam, S., Zarraga, G., Colby, G., Baltier, K., et al. (2015). The BioPlex Network: A Systematic Exploration of the Human Interactome. Cell *162*, 425–440.

The American Journal of Human Genetics, Volume *99*

Supplemental Data

TTC25 Deficiency Results in Defects of the Outer Dynein Arm Docking Machinery and Primary Ciliary Dyskinesia with Left-Right Body Asymmetry Randomization

Julia Wallmeier, Hidetaka Shiratori, Gerard W. Dougherty, Christine Edelbusch, Rim Hjeij, Niki T. Loges, Tabea Menchen, Heike Olbrich, Petra Pennekamp, Johanna Raidt, Claudius Werner, Katsura Minegishi, Kyosuke Shinohara, Yasuko Asai, Katsuyoshi Takaoka, Chanjae Lee, Matthias Griese, Yasin Memari, Richard Durbin, Anja Kolb-Kokocinski, Sascha Sauer, John B. Wallingford, Hiroshi Hamada, and Heymut Omran

Supplemental Material:

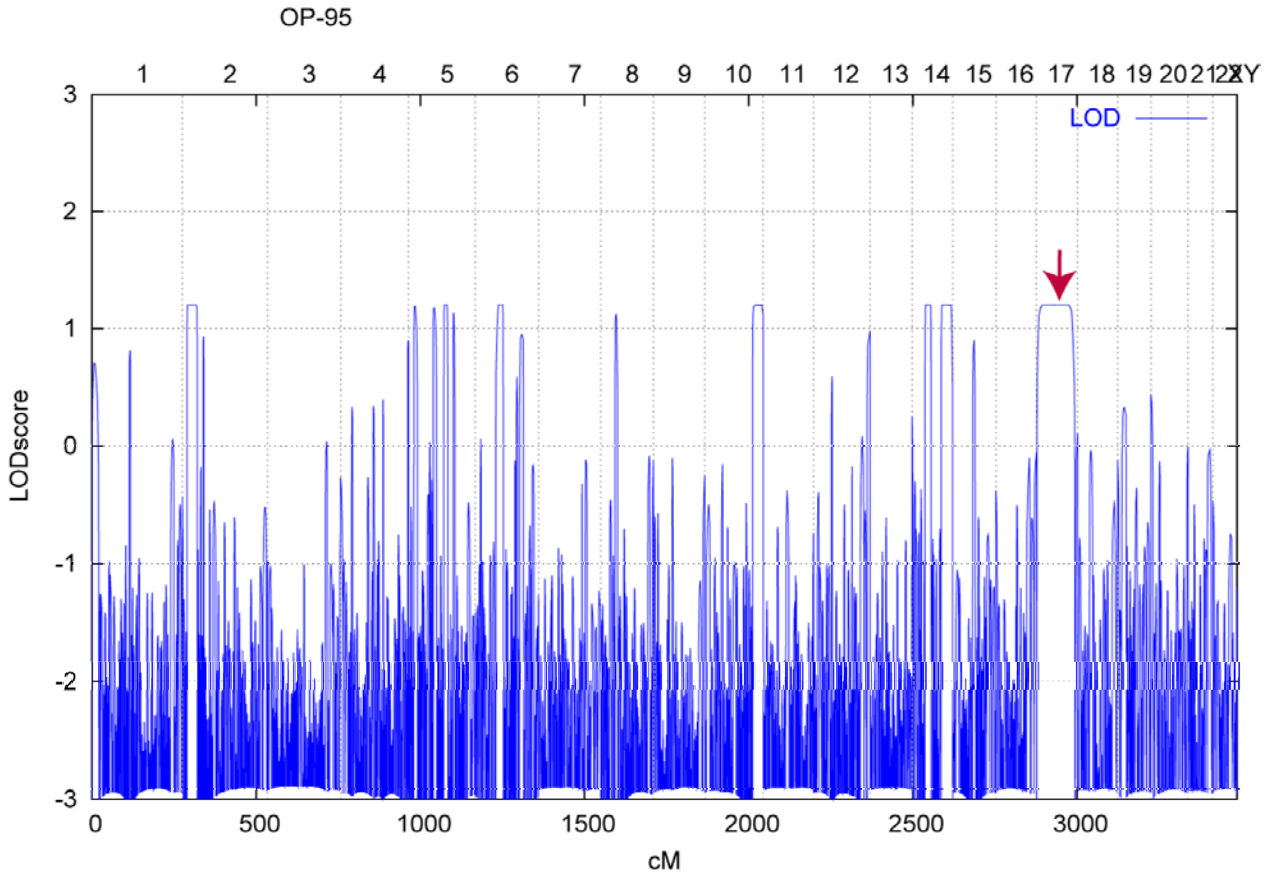

Figure S1: SNP-Haplotype analysis of OP-95 II1; cM: centimorgan, Allegro LOD score: logarithm of the odds

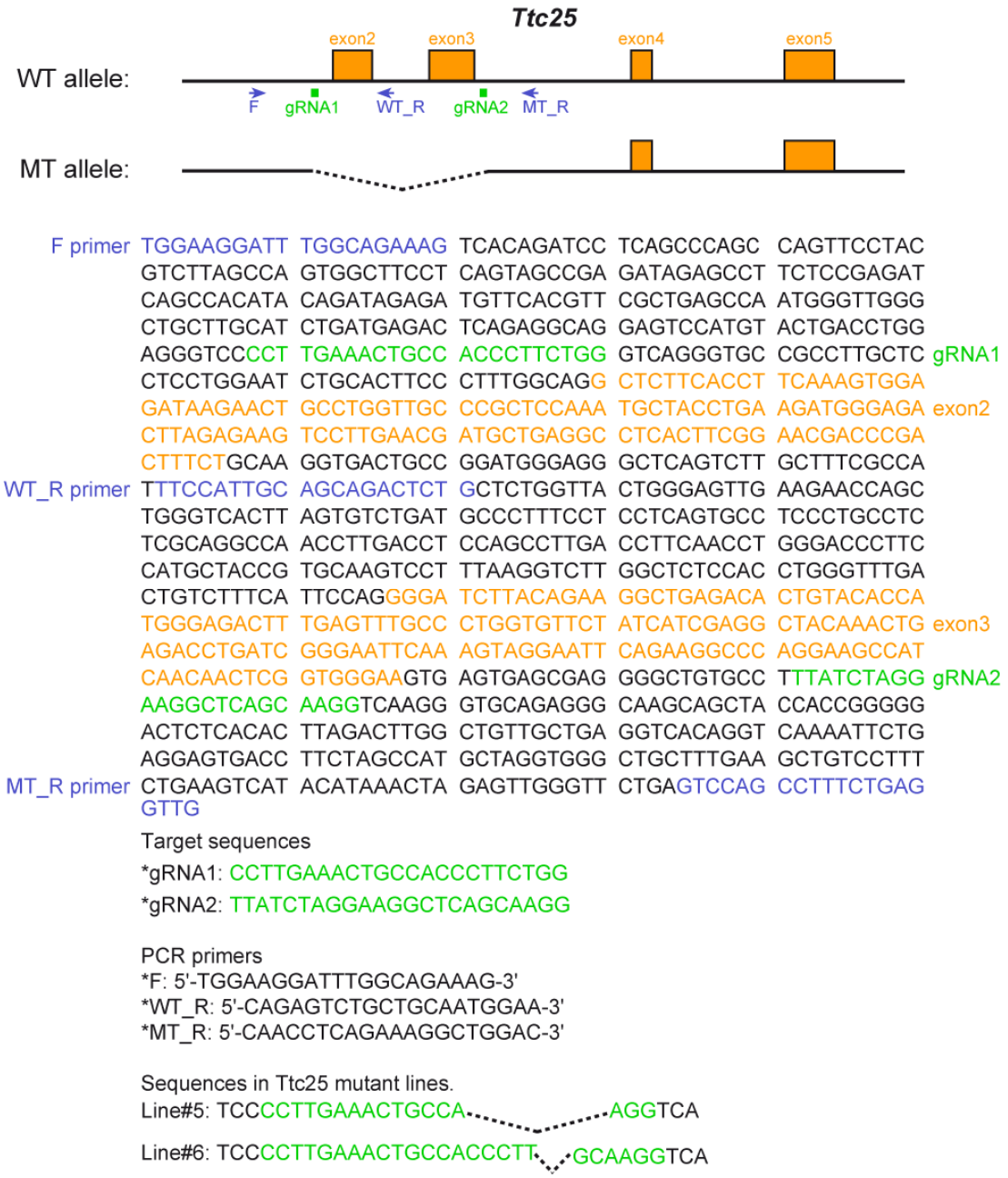

Figure S2: Generation of mutant mice by CRISPR/Cas9 system.

Ttc25 mutant mice were generated with the use of the clustered regularly interspersed short palindromic repeats (CRISPR)/Cas9 system. Two small guide RNAs (sgRNAs) designed to delete *Ttc25* exons 2 and 3 were produced by *in vitro* transcription (IVT) with the use of a MEGA short script T7 kit (Ambion, AM1354) essentially as previously described. Capped synthetic mRNA for Cas9 was transcribed from the Cas9/pSP64T vector with the use of an SP6 mMessage mMachine Kit (Ambion, AM1340). Cas9 mRNA and the two sgRNAs were injected into C57BL/6 fertilized eggs as previously described[24]. The pups were genotyped by polymerase chain reaction (PCR) and subsequent sequence analysis. The primers used were F: 5'-TGGAAGGATTTGGCAGAAAG and MT_R: 5'-CAACCTCAGAAAGGCTGGAC.

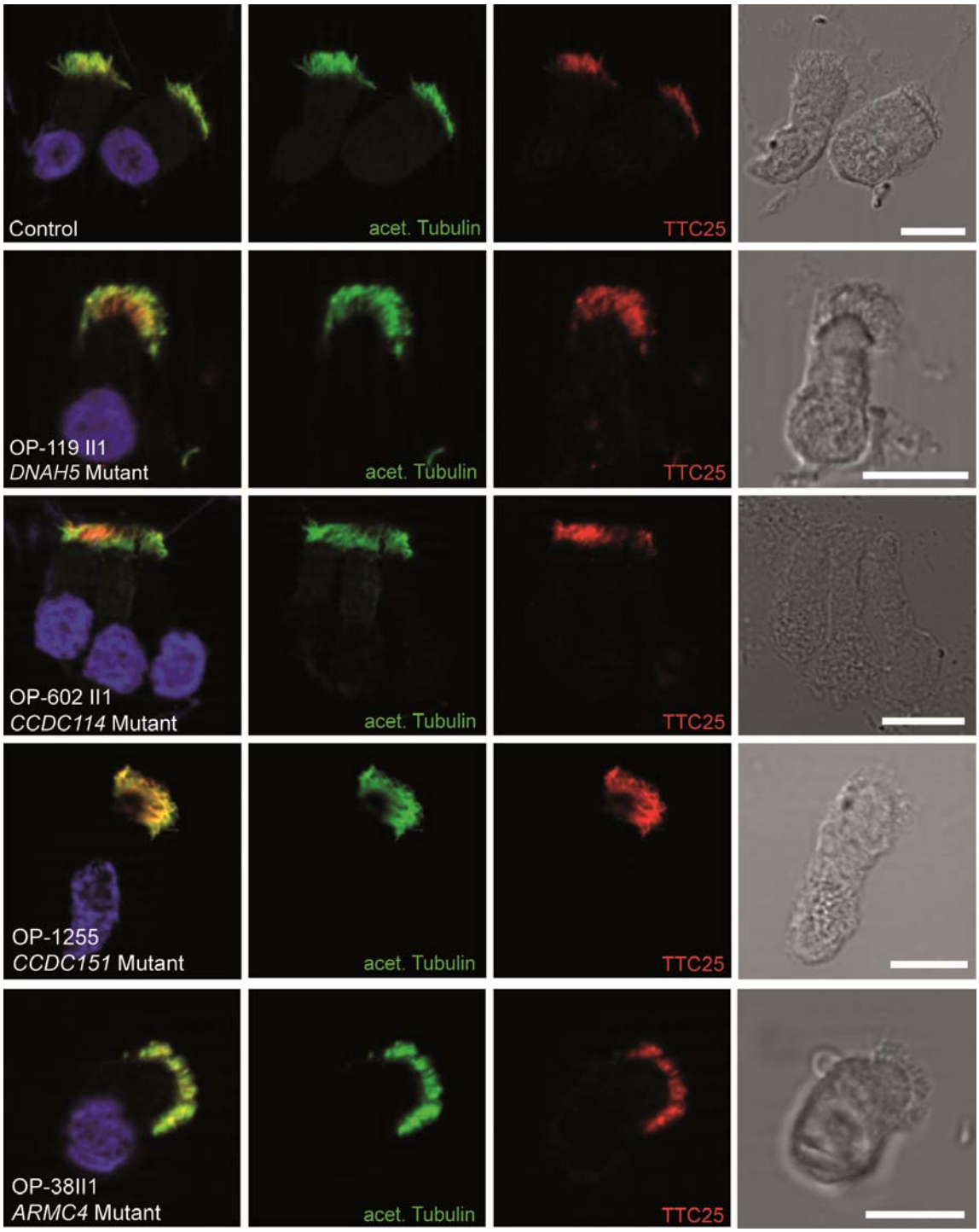

Figure S3: TTC25 is detectable in ODA-HC and ODA-DC mutant cilia.

Respiratory cilia from control and PCD individual (OP-119 II1) carrying *DNAH5* LOF-mutations were double labeled with antibodies directed against acetylated Tubulin and TTC25. Respiratory cilia from control and PCD individuals with ODA-DC defects carrying LOF-mutations in *CCDC114* (OP-602 II1), *CCDC151* (OP-1255) and *ARMC4* (OP-38 II1) respectively were double labeled with antibodies directed against acetylated tubulin and TTC25. Yellow color represents co-localization of TTC25 and acetylated tubulin. Nuclei (blue) were stained with Hoechst33342. Scale bars represent 10µm.

Table S1: Rare variants in the homozygous region (17:5961695-78901893) of OP-95II1 (Frameshift, Splice site-Substitution, Non-Synonymous Substitution, Variation frequency <0.005)

Gene	Ensembl gene number	cDNA level	Protein level	Variation	Variation frequency
MYH4	ENSG00000264424	c.3833C>T	p.S1278L	rs145453135	0.0003
NT5M	ENSG00000205309	c.604_615del(CTGCAG)2ins(CTGCAG)3	p.Q205_P206insLQ	n.a.	n.a.
PHF12	ENSG00000109118	c.1534C>G	p.H512D	n.a.	n.a.
GIT1	ENSG00000108262	c.1489G>A	p.A497T	n.a.	n.a.
SLFN11	ENSG00000172716	c.766G>A	p.E256K	n.a.	n.a.
SLFN12	ENSG00000172123	c.42G>C	p.L14F	rs202085233	0.0002
KRTAP29-1	ENSG00000212658	c.833A>G	p.K278R	n.a.	n.a.
KRT32	ENSG00000108759	c.665C>G	p.S222C	n.a.	n.a.
TTC25	**ENSG00000204815**	**c.114+1G>T**	**Splice site**	**n.a.**	**n.a.**
INTS2	ENSG00000108506	c.380C>T	p.T127M	rs370752436	0.0002
CASKIN2	ENSG00000177303	c.2635G>A	p.V879I	n.a.	n.a.
GALR2	ENSG00000182687	c.1163G>C	p.*388S	n.a.	n.a.

n.a.: not available

Table S2: Rare variants in the shared homozyous region (17:16479171-66815637) of OP-1331 II1 and II2 (Frameshift, Splicesite-Substitution, Non-Synonymous Substitution, Variation frequency <0.005).

Gene	Ensembl gene number	cDNA level	Protein level	Variation	Variation frequency
EVI2A	ENSG00000126860	c.494C>A	p.S165Y	rs147909684	0.0003
C17orf50	ENSG00000154768	c.374G>A	p.R125Q	n.a	n.a
KRTAP1-1	ENSG00000188581	c.125C>T	p.T42I	n.a	n.a
TTC25	**ENSG00000204815**	**c.425_426insT**	**p.K142Nfs*12**	**n.a**	**n.a**
KCNH4	ENSG00000089558	c.2696G>A	p.R899Q	n.a	n.a
FAM187A	ENSG00000214447	c.-1466+6T>A	Splice site	n.a	n.a
COPZ2	ENSG00000005243	c.16-1delCins(C)2	Splice site	n.a	n.a
XYLT2	ENSG00000015532	c.1942-8_23del(TTTA)4ins(TTTA)3	Splice site	n.a	n.a
EME1	ENSG00000154920	c.567T>A	p.N189K	rs150118812	0.0012
LRRC59	ENSG00000108829	c.126A>T	p.N43I	rs150118812	0.0012
MTMR4	ENSG00000108389	c.3029A>G	p.D1010G	rs61742345	0.000099

n.a.: not available

Table S3: Phenotype in TTC25 mutant mice (2 weeks old)

	1	**2**	**3**	**4**	**5**	**6**
Heart apex on the right side	x	-	x	x	x	-
Reversed lung lobation	x	-	x	x	x	-
Aortic arch on the right side	x	-	x	x	x	-
Azygos vein on the right side	x	-	x	x	x	-
Stomach on the right side	x	-	x	-	x	-
Abnormal liver lobation	ND	x	ND	-	x	-
Vena cava located to the left of the aorta	-	x	ND	-	-	-
Slow moving of tracheal cilium	ND	x	ND	x	x	x
Hydrocephalus	ND	ND	ND	x	x	-
Small body	ND	x	x	x	x	x

X: defect is present; -: defect is absent; ND: not determined

Table S4: Genotypes from intercross of *Ttc25*+/- mice (2 weeks-old)

Line No.	*Ttc25* +/+ (%)	*Ttc25* +/- (%)	*Ttc25* -/- (%)	Total
#5	13 (33.3%)	22 (56.4%)	4 (10.3%)	39 (100%)
#6	5 (35.7%)	7 (50.0%)	2 (14.3%)	14 (100%)

+/+: wild type; *Ttc25* +/-: heterozygous;*Ttc25* -/-: homozygous

Supplemental References:

24. Saijoh, Y., Adachi, H., Mochida, K., Ohishi, S., Hirao, A., and Hamada, H. (1999). Distinct transcriptional regulatory mechanisms underlie left-right asymmetric expression of lefty-1 and lefty-2. Genes Dev. *13*, 259–269.